ELSEVIER

International Journal of Heat and Fluid Flow 23 (2002) 186–193

International Journal of HEAT AND FLUID FLOW

www.elsevier.com/locate/ijhff

Heat transfer in transitional and turbulent boundary layers with system rotation

D. Yamawaki, S. Obi, S. Masuda *

Department of Mechanical Engineering, Faculty of Science and Technology, Keio University, 3-14-1 Hiyoshi, Kohoku-ku, Yokohama 223-8522, Japan

Abstract

The present paper reports on the influence of system rotation on the heat transfer characteristics of transitional and turbulent zero-pressure gradient boundary layers. A test plate is installed in a wind tunnel, which is rotatable around the axis parallel to the plate leading edge with constant speed of rotation. Local heat transfer coefficient during rotation is determined by employing a thermochromic liquid crystal. Effects of the Coriolis force and the centrifugal buoyancy force have been examined by comparing the heat transfer coefficient with different free-stream velocities, rotational speeds and wall temperatures. It has been revealed that the Coriolis force has significant effect on transitional heat transfer, while its effect on turbulent heat transfer is moderate. The centrifugal buoyancy exhibits additional effects if the thermal loading is high.

Keywords: Heat transfer; Flat plate boundary layer; System rotation; Coriolis force; Centrifugal buoyancy; Goertler instability; Liquid crystal

1. Introduction

A fundamental knowledge of the heat transfer characteristics in rotating boundary layers is necessary for an optimum design of a cooling system in a rotating machinery. Although there are a lot of investigations on the heat transfer in rotating ducts, as reviewed by Edo et al. (2000), most of their geometries are too complicated to clarify the individual effects such as Coriolis force, centrifugal buoyancy force, secondary flow, corner vortices, curvature of duct center line and so on. Future development of heat transfer augmentation technology will require more sophisticated devices depending on the dynamical situations of each wall, for which information on the individual effects are necessary.

The influence of the pure Coriolis force normal to the wall has been reported by Matsubara and Alfredsson (1996) for a rotating channel flow and Edo et al. (2000) for a rotating flat plate boundary layer. Both of them showed that the heat transfer coefficient is dramatically increased when the streamwise vortex instability breaks out. Their investigations, however, are limited only to the laminar and transitional layers for low thermal loading, in which the effect of the centrifugal buoyancy is negligible.

The present investigation is an extension of Edo et al. (2000) to the turbulent boundary layer including high thermal loading condition. Unlike the laminar and transitional boundary layers, the turbulent heat transfer is multiply influenced by the system rotation, through the turbulent mixing of momentum and energy in addition to the mean Coriolis force. Further, if the temperature difference is large, the effect of centrifugal buoyancy may become important.

The schematic view of the present problem and the definition of the coordinate system are given in Fig. 1. The test plate is installed in the wind tunnel, which is rotatable around the orthogonal axis with constant speed of rotation. The leading edge of the test plate is aligned with the axis of system rotation and thus Coriolis force acts normal to the surface, while its direction depends on the direction of rotation. Under the constant heat flux condition, the local heat transfer coefficients are measured by changing the free-stream velocity, the direction and speed of system rotation as well as the temperature difference between the wall surface and the free-stream. They are expressed as a function of Reynolds number and rotation number and compared with the existing stationary data.

* Corresponding author. Tel.: +81-45-566-1517; fax: +81-45-566-1517.

E-mail address: smasuda@mech.keio.ac.jp (S. Masuda).

0142-727X/02/$ - see front matter
PII: S0142-727X(01)00148-5

Nomenclature

A	surface area of the heater
C_p	specific heat at constant pressure
E	voltage supplied to the heater
h_x	local heat transfer coefficient ($\equiv (q - q_{loss})/(T_w - T_\infty)$)
I	current supplied to the heater
k	thermal conductivity of the fluid
L	reference length (length of the heater)
Nu_x	local Nusselt number ($\equiv h_x x/k$)
Pr	Prandtl number ($\equiv \mu C_p/k$)
q	heat flux given to the heater ($\equiv IE/A$)
q_{loss}	heat loss due to conduction and radiation
r_i	position vector
R	radial distance to the plate leading edge
Ra_Ω	rotational Rayleigh number ($\equiv \beta\Omega^2(T_w - T_\infty)L^4/(\nu\alpha)$)
Re_x	local Reynolds number ($\equiv \rho U_\infty(x - x_0)/\mu$)
Re_L	bulk Reynolds number ($\rho U_\infty L/\mu$)
Ro_L	bulk Rotation number ($\equiv \Omega L/U_\infty$)
St_x	Stanton number ($\equiv h_x/\rho C_p U_\infty$)
T	temperature relative to the reference value
T_w	local wall temperature
T_∞	free-stream temperature
t	fluctuating temperature
U	mean streamwise velocity
U_i	mean velocity components
u_i	fluctuating velocity components
U_∞	free-stream velocity
$(x, y, z), x_i$	rotating coordinate system
x_0	x at leading edge of the heater

Greeks

α	thermal diffusivity
β	volume expansion coefficient
δ	momentum boundary layer thickness
δ_T	thermal boundary layer thickness
ε_{ijk}	Eddington's tensor
ϕ	centrifugal force potential
ν	kinematic viscosity
ρ	fluid density
τ	time
Ω, Ω_i	angular velocity of system rotation
$*$	denotes instantaneous values

There are a number of investigations on the isothermal Goertler instability in a laminar boundary layer over a stationary concave wall. Although the centrifugal force instead of Coriolis force drives the instability, the underlying concept is the same as the present. The extensive review has been given by Saric (1994). Non-isothermal flow over a concave wall has been investigated by Liu and Lee (1995). They present the numerical simulation on the heat-transfer problem in a nonlinearly developing longitudinal vortex system that arose from upstream weak Goertler vortices. Crane and Sabzvari (1989) and Toe et al. (2001) conducted the heat transfer experiment in concave wall boundary layers.

2. Theoretical considerations

2.1. Vorticity aspects

We consider the non-inertial reference frame x_i, which is rotating with constant angular velocity Ω_i. The conservation equations of mass and energy remain the same as in the inertial reference frame, while the conservation equations of momentum and vorticity contain the additional terms associated with the system rotation.

In the framework of the Boussinesq approximation, the additional terms in the relative vorticity equation can be written as

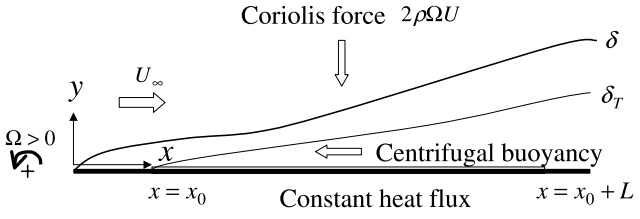

Fig. 1. Schematic view of rotating boundary layer and definition of coordinate system (pressure surface).

$$f^*_{\omega i} = 2\Omega_l \frac{\partial u^*_i}{\partial x_l} + \beta\varepsilon_{ilm}\frac{\partial}{\partial x_l}\left(t^*\frac{\partial \phi}{\partial x_m}\right). \quad (1)$$

In this equation, u^*_i denotes the x_i-component of the instantaneous velocity relative to the non-inertial frame, t^* is the instantaneous temperature relative to the reference condition, β is the volume expansion coefficient of the fluid, ε_{ijk} is Eddington's tensor and ϕ indicates the centrifugal force potential defined as,

$$\varepsilon_{ijk}\varepsilon_{klm}\Omega_j\Omega_l r_m \equiv \frac{\partial \phi}{\partial x_i}, \quad (2)$$

where r_i denotes the position vector with respect to the axis of the system rotation.

The first and second terms on the right-hand side of Eq. (1) represent the vorticity sources due to the Coriolis acceleration and the centripetal acceleration, respectively. The latter is called centrifugal buoyancy effect, which may be important when the thermal loading is

Table 1
Vorticity sources arising from system rotation (x_3 coincides with the axis of rotation)

Variable	Coriolis	Centrifugal buoyancy
ω_1^*	$+2\Omega_3(\partial u_1^*/\partial x_3)$	$+\beta\Omega_3^2 r_2(\partial t^*/\partial x_3)$
ω_2^*	$+2\Omega_3(\partial u_2^*/\partial x_3)$	$-\beta\Omega_3^2 r_1(\partial t^*/\partial x_3)$
ω_3^*	$+2\Omega_3(\partial u_3^*/\partial x_3)$	$+\beta\Omega_3^2(r_2(\partial t^*/\partial x_1) - r_1(\partial t^*/\partial x_2))$

high. Since the energy equation does not contain the rotational terms explicitly, laminar and transitional heat transfer is affected by the system rotation only indirectly through the convection which is modified by the rotational terms given in Eq. (1).

If the x_3 axis is chosen parallel to the axis of rotation as shown in Fig. 1, these terms can be reduced as listed in Table 1. The essential ability of Coriolis force to generate streamwise vortices for positive Ω_3 is understood if we refer to the Coriolis term in the ω_1-equation. In this coordinate system, this term has positive contribution to $D\omega_1/D\tau$ in the region of the positive gradient $\partial u_1/\partial x_3$ and vice versa for the negative gradient. Thus a single infinitesimal hump of initial spanwise velocity profile tends to induce a pair of counterrotating vortices. The resulting upwash and downwash further enhance the spanwise non-uniformity and again contribute to build up the streamwise vortices. This sequence of events does not continue unlimitedly because the Coriolis source terms in ω_2- and ω_3-equations contribute to resist the unlimited growth of ω_1 and eventually reaches the equilibrium state, which we recognize as the steady streamwise vortex systems. They may contribute to the transport of heat in the wall-normal direction.

By inspecting the sign of the centrifugal buoyancy terms given in Table 1, it may be inferred that they further promote the generation of streamwise vortices if the wall is cooled and vice versa if the wall is heated. It is also important to note that, for negative Ω_3, this sequence of events does not exist at all because the upwash and downwash due to streamwise vortices, if they were generated, wipe out the initial non-uniformity and the boundary layer tends to become two-dimensional.

2.2. Turbulent heat transfer

Although the vorticity considerations mentioned above are also applicable to the instantaneous velocity field of turbulent boundary layers, the situation is much more complicated and the best way to understand the turbulent heat transfer is to consult with the Reynolds averaged energy equation,

$$\frac{\partial T}{\partial \tau} + \frac{\partial U_l T}{\partial x_l} = \alpha \frac{\partial^2 T}{\partial x_l \partial x_l} - \frac{\partial \overline{u_l t}}{\partial x_l}, \tag{3}$$

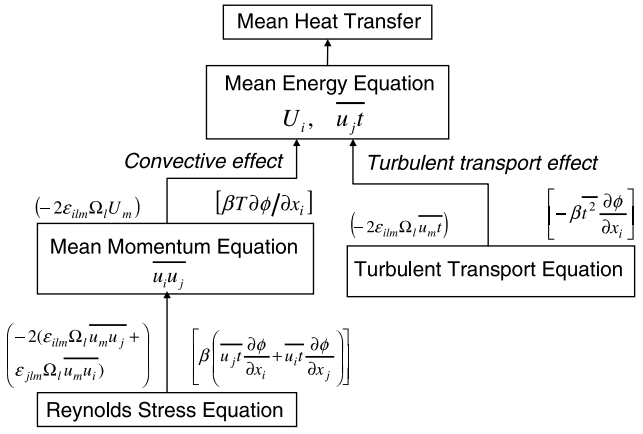

Fig. 2. System of governing equations for turbulent heat transfer in rotating frame of reference. ( ) Coriolis term, [ ] centrifugal buoyancy term.

where T and t are the mean and fluctuating temperatures, U_l denotes the mean streamwise velocity, τ denotes time and α denotes the thermal diffusivity. Although this equation does not contain the rotational term explicitly, the mean temperature distribution is affected indirectly by the system rotation via convective and diffusive effects as illustrated in Fig. 2. The Coriolis terms are given in the round brackets and the centrifugal buoyancy terms are given in the square brackets. Their specific forms are tabulated in Table 2.

The primary diffusion term in Eq. (3), $-\partial\overline{u_2 t}/\partial x_2$, is affected by rotation through the Coriolis term $+2\Omega_3\overline{u_1 t}$ and the centrifugal buoyancy term $+\beta\Omega_3^2 r_2\overline{t^2}$, both appearing in the $(-\overline{u_2 t})$-equation. If we assume $\overline{u_1 t}$ to be of the same order of magnitude as $\overline{u_2 t}$, $+2\Omega_3\overline{u_1 t}$ may have significant contribution to the change of $\overline{u_2 t}$, while $+\beta\Omega_3^2 r_2\overline{t^2}$ may be negligible, since $r_2 \approx O(\delta)$. Thus the contribution of system rotation through turbulent diffusion may become important for the high speed of rotation and its effect may depend on the direction of rotation.

The convective effect is brought about primarily by the Reynolds shear stress $-\overline{u_1 u_2}$. When $\Omega_3 > 0$, the Coriolis source term $2\Omega_3(\overline{u_1^2} - \overline{u_2^2})$ has a positive con-

Table 2
Specific form of source terms arising from system rotation for 2D turbulent flow (x_3 is the same as Table 1)

Variable	Coriolis	Centrifugal buoyancy
U_1	$+2\Omega_3 U_2$	$-\beta\Omega_3^2 r_1 T$
U_2	$-2\Omega_3 U_1$	$-\beta\Omega_3^2 r_2 T$
T	–	–
$-\overline{u_1 u_2}$	$+2\Omega_3\left(\overline{u_1^2} - \overline{u_2^2}\right)$	$+\beta\Omega_3^2(r_1\overline{u_2 t} + r_2\overline{u_1 t})$
$\overline{u_1^2}$	$+4\Omega_3\overline{u_1 u_2}$	$-2\beta\Omega_3^2 r_1\overline{u_1 t}$
$\overline{u_2^2}$	$-4\Omega_3\overline{u_1 u_2}$	$-2\beta\Omega_3^2 r_2\overline{u_2 t}$
$\overline{u_3^2}$	–	–
$-\overline{u_1 t}$	$-2\Omega_3\overline{u_2 t}$	$+\beta\Omega_3^2 r_1\overline{t^2}$
$-\overline{u_2 t}$	$+2\Omega_3\overline{u_1 t}$	$+\beta\Omega_3^2 r_2\overline{t^2}$

tribution to the Reynolds shear stress $-\overline{u_1 u_2}$, since usually $\overline{u_1^2} > \overline{u_2^2}$, although this contribution is reduced by the Coriolis terms in the $\overline{u_1^2}$- and $\overline{u_2^2}$-equations. For a strongly heated wall, the centrifugal buoyancy term $\beta\Omega_3^2 r_1 \overline{u_2 t}$ also helps the Reynolds stress production. For $\Omega_3 < 0$, the latter effect remains the same, while the Coriolis source term absolves the Reynolds stress. Some of the previous investigations showed that the centrifugal buoyancy enhances the heat transfer (Morris and Ayhan, 1979; Wagner et al., 1991). However, it is not so straightforward and the final results depend on the relative magnitude of the related terms. The correct answer for this question can only be provided after conducting well-controlled experiments or numerical simulations.

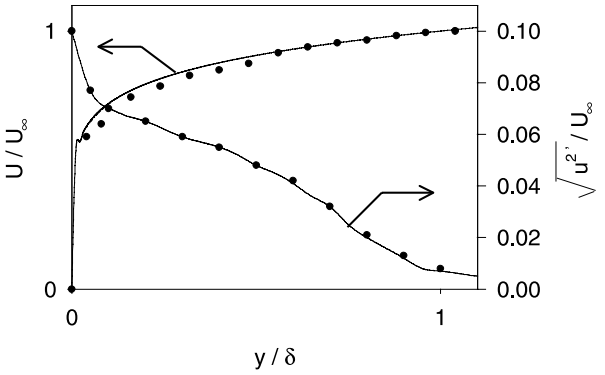

Fig. 4. Mean and rms velocity distributions at the leading edge of the heater without rotation (solid lines are the standard data by Klebanoff (1955)).

3. Experimental Method

The experimental apparatus used in the present study is essentially the same as that of the previous paper (Edo et al., 2000). As illustrated schematically in Fig. 1, a 10 mm thick acrylic test plate with elliptic leading edge is inserted into a wind tunnel of $760 \times 86 \times 390$ mm^3, which can rotate around the spanwise axis with changing direction and speed of rotation up to 20 rad/s. A stainless foil heater of length $L = 500$ mm is glued onto the test surface, whose leading edge is located at $x = 150$ mm ($=x_0$), x being the downstream distance from the plate leading edge. For the turbulent experiment, a tripping wire of 3 mm diameter is attached at $x = 30$ mm. The standard velocity profiles for laminar and turbulent flat plate boundary layers have been confirmed at the leading edge of the heater as shown in Figs. 3 and 4.

The wall temperature distributions are obtained by employing a thermochromic liquid crystal sheet of 0.05 mm thick attached onto the foil heater by the adhesive tape of 0.01 mm thick. The calibration correlating the hue values of the color picture obtained by a CCD camera and the wall temperature is conducted by keeping the lighting and photographing conditions as identical as possible to the actual measurement. The temperature sensitive range is from 300 to 311 K. The spatial resolution depends on the photographic condition, with the typical value being 0.6 mm. The total error of the temperature measurement with liquid crystal was estimated to be approximately ± 0.3 °C. For the high thermal loading experiment, the wall temperature was obtained by employing 20 CC-thermocouples distributed just beneath the foil heater, since the temperature to be measured is out of range of the liquid crystal. The heat flux is evaluated from the electric power supplied to the heater divided by the area covered by the heater. The heat conduction loss to the solid wall has been compensated by measuring temperature at the back of the test plate by employing 28 embedded thermocouples. Heat loss by radiation is neglected.

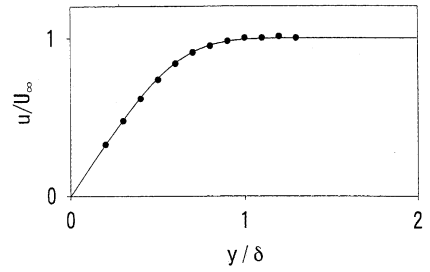

Fig. 3. Velocity distribution at the leading edge of the heater without rotation (solid line indicates Blasius profile).

The mean velocity distribution and its fluctuation are measured by employing single constant temperature hot-wire with the heater off. We assume that the same velocity profiles would be obtained with the heater on. In the transitional flow experiment, an array of tiny humps is fitted in order to reproduce the same spanwise position of the streamwise vortices. The spanwise pitch of the humps is set equal to the average wavelength observed in the natural transition experiment (Masuda et al., 1994). The size of the humps has been made so small that the spanwise velocity non-uniformity is not observed when without the system rotation. It has been confirmed the free stream turbulence level is around one percent. The traverses of the hot wire probe and the CC-thermocouple in cross-stream planes give the contours of the mean velocity and its fluctuation as well as the fluid temperature. The traversing, the data acquisition and the video recording are implemented remotely from the stationary frame by supplying the power and transmitting the signals via mercury slip rings. In order to detect the wall, a thin needle is attached to the probe stem, which determines the minimum distance from the wall to be 0.3 mm. Further details are given in Edo et al. (2000).

4. Results and discussion

4.1. Low thermal loading experiments

In Fig. 5, the local Stanton number $St_x \equiv h_x/\rho C_p U_\infty$ on the pressure surface together with the stationary case is presented as a function of the local Reynolds number $Re_x \equiv U_\infty(x - x_0)/v$ for $T_w - T_\infty = 10$ K . In this case, the test plate is rotating in the direction illustrated in Fig. 1 and thus $\Omega > 0$. h_x is the local heat transfer coefficient, ρ and C_p are the density and specific heat at constant pressure, U_∞ is the free-stream velocity, x_0 is the streamwise distance from the leading edge of the heater, T_w is the spanwise average of the wall temperature and T_∞ is the free-stream temperature. For this temperature condition, the centrifugal buoyancy effect is considered to be negligible. The bulk Reynolds number $Re_L \equiv (U_\infty L/v) = 2.3 \times 10^5$ and the rotation number is defined as $Ro_L \equiv \Omega L/U_\infty$, where L is the length of the heater. For the stationary case, the present results after heat loss compensation coincide with the values deduced from the following empirical formulas for laminar boundary layers by Lighthill (1950) and turbulent boundary layers by Reynolds et al. (1958) within 3% deviations, showing the soundness of the present experimental method.

$$Nu_x = 0.453 Pr^{1/3}(Re_x + Re_{x0})^{1/2}\left[1 - (x_0/x)^{3/4}\right]^{-1/3} \quad \text{(laminar)}, \tag{4}$$

$$Nu_x = \frac{0.0296 Pr^{3/5}(Re_x + Re_{x0})^{4/5}}{\left[1 - (x_0/x)^{9/10}\right]^{1/9}}\left(\frac{T_w}{T_\infty}\right)^{0.4} \quad \text{(turbulent)}. \tag{5}$$

In the above equations, Re_{x0} is the Reynolds number based on x_0, the length of the non-heated portion of the plate.

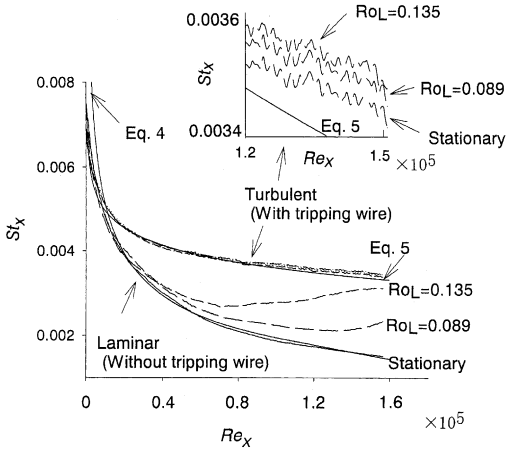

Fig. 5. Stanton number distribution in pressure side boundary layer with low thermal loading ($U_\infty = 7$ m/s, $T_w - T_\infty = 10$ K).

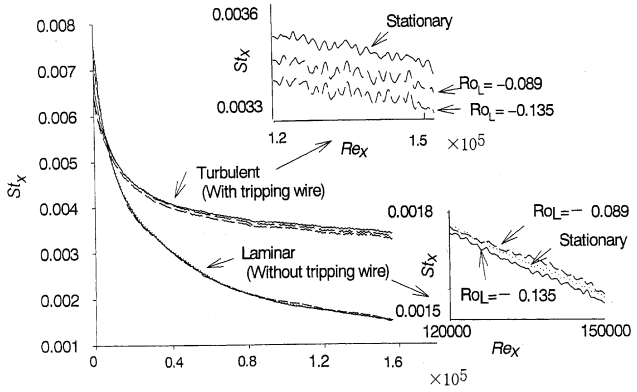

Fig. 6. Stanton number distribution in suction side boundary layer with low thermal loading ($U_\infty = 7$ m/s, $T_w - T_\infty = 10$ K).

The data without tripping wire reveal that the heat transfer in the laminar boundary layer is dramatically augmented compared with the stationary case especially in the downstream region, the gain increasing with the rotational speed. The data with tripping wire, on the other hand, show only a slight increase of St_x with increasing speed of rotation as shown in the enlarged picture. Though not shown here, the difference increases with decreasing free-stream velocity, suggesting the increase of relative importance of the Coriolis effect comparative to the inertial effect.

The results of similar experiment but with opposite direction of rotation are given in Fig. 6. The direction of Coriolis force in this arrangement is away from the test surface (suction surface) and the boundary layer is expected to be stabilized. The results without tripping wire exhibit no systematic change with rotation even in the enlarged picture. This rotation independence is naturally understood if we consider that the rotational effect in a low temperature laminar boundary layer is solely due to the vorticity sink in Eq. (1) and thus the flow field tends to remain two-dimensional and steady as explained in Section 2.1.

The results with tripping wire are also shown in Fig. 6, which indicate a slight decrease of St_x with increasing speed of rotation. In contrast to the laminar case, the turbulent heat transfer is multiply affected by the Coriolis force as shown in Fig. 2 and Table 2. The attenuation of heat transfer presented here may be the indirect consequence of the Coriolis sink in the Reynolds shear stress equation.

4.2. Temperature and velocity fields

For the transitional boundary layer on the pressure surface, the iso-velocity contours in the cross-stream plane at $x = 330$ mm (Fig. 7(a)) are compared with those of temperature (Fig. 7(b)). Both contours exhibit the identical mushroom shapes generated by the streamwise

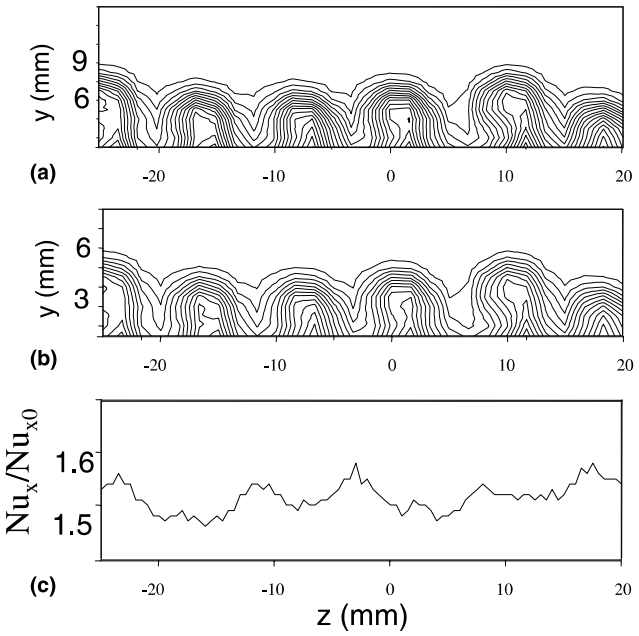

Fig. 7. (a) Iso-velocity contour, (b) iso-temperature contours and (c) spanwise distribution of local Nusselt number in transitional boundary layer on pressure surface ($U_\infty = 4$ m/s, $x = 330$ mm, $\Omega = 4.1$ rad/s, $\Delta T = 10$ K, without tripping wire, Contour spacing is 0.05 in u/U_∞ and 0.1 in $(T - T_\infty)/(T_w - T_\infty)$, Nu_{x0} is the local Nusselt number for a stationary case).

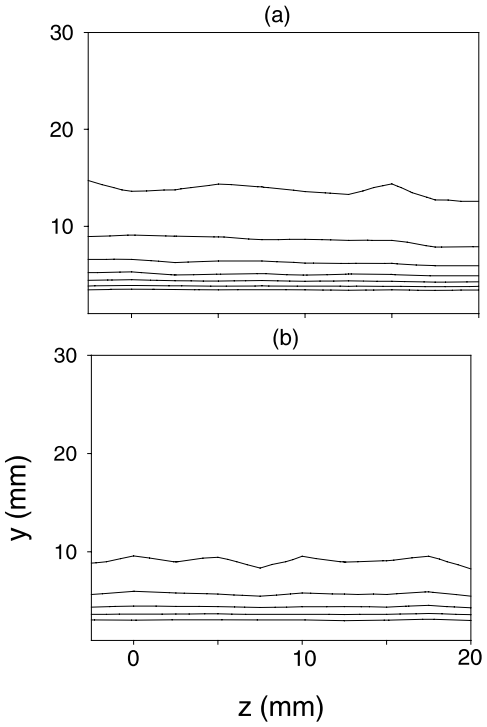

Fig. 8. (a) Iso-velocity and (b) iso-temperature contours in turbulent boundary layer on pressure surface ($U_\infty = 4$ m/s, $x = 330$ mm, $\Omega = 4.1$ rad/s, $\Delta T = 10$ K, with tripping wire, Contour spacing is 0.075 in u/U_∞ and 0.1 in $(T - T_\infty)/(T_w - T_\infty)$).

vortices due to Goertler instability. The spanwise distribution of local Nusselt number given in Fig. 7(c) is closely related to this streamwise vortical structure. The spanwise regions of the minimum Nusselt number correspond to the upwash region, where the heated fluid is accumulated along the surface. This reduces the local temperature difference $T_w - T_\infty$, and combined with the thicker boundary layer there, the local minimum of the Nusselt number has resulted. In the downwash region, on the other hand, the colder fluid is coming from the free stream, and the boundary layer is thinner, resulting in the local maximum of Nusselt number. These increase and decrease of the near wall temperature are not mutually cancelled out, resulting in the increase of spanwise-mean heat transfer coefficient as seen in Fig. 5. As mentioned in Section 2.2, only the Coriolis force term in the momentum equation is responsible for the low temperature laminar and transitional heat transfer. This convective effect actually influences the transitional heat transfer as seen here. These results are essentially similar to those by Matsubara and Alfredsson (1996) in the pressure side boundary layer as well as by Crane and Sabzvari (1989) and Toe et al. (2001) in the concave wall boundary layers. There is absolutely no such kind of effect in the suction surface boundary layer.

In Fig. 8, the cross-stream distributions of mean velocity and temperature for turbulent boundary layer on pressure surface are shown. In contrast to the transitional boundary layer, the mean flow field of the turbulent boundary layer remains two-dimensional without any indication of the streamwise vortices. This fact suggests that the main contribution of Coriolis force on turbulent heat transfer is not through the Coriolis term in the mean momentum equation but through the Coriolis source terms in the Reynolds stress equation and in the turbulent transport equation due to the modification of turbulent eddies by fluctuating Coriolis force.

4.3. Effect of centrifugal buoyancy

To evaluate the effect of centrifugal buoyancy on the turbulent heat transfer, the heat transfer coefficient was measured by carefully increasing the wall temperature T_w, while the free-stream velocity and the rotational speed were kept constant. Fig. 9 shows the local Nusselt number Nu_x for three cases of rotation. The data were obtained at $x = 530$ mm and the free stream velocity equal to 4 m/s. Nu_x is normalized by the corresponding value Nu_{x0} without rotation at $\Delta T = 10$ K.

For each constant-Ω curve, the Coriolis force remains constant, while the centrifugal buoyancy force varies with ΔT. The curves for $\Omega = \pm 6.28$ rad/s indicate a gradual increase of the Nusselt number, showing that the centrifugal buoyancy promotes turbulent heat

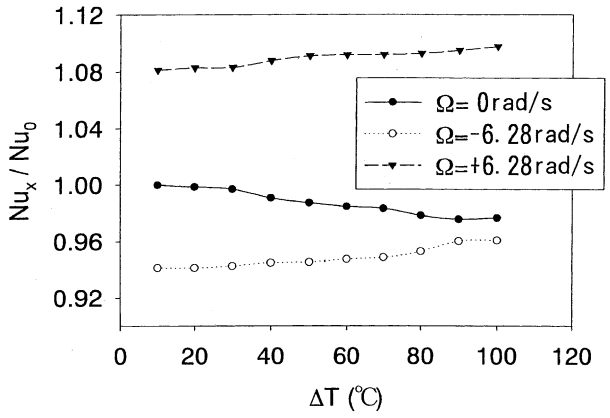

Fig. 9. Effect of centrifugal buoyancy on turbulent heat transfer ($U_\infty = 4$ m/s, $x = 530$ mm, with tripping wire).

transfer independent of the directions of rotation. The gradual decrease seen in the stationary curve suggests that there are some defects in the surface temperature measurement or in the heat loss correction. Providing the same magnitude of error for rotating cases, the increase by the effect of centrifugal buoyancy is estimated approximately as 4% in both directions of rotation. Although this increase is smaller than that of Coriolis effects at least in the present range of experiment, it may become increasingly important for high thermal loading.

As mentioned in Section 2.2, the buoyancy source term $\beta r_2 \Omega_3^2 \overline{t^2}$ in the $(-\overline{u_2 t})$-equation is small for thin boundary layer, while the buoyancy source term $\beta r_1 \Omega_3^2 \overline{u_2 t}$ in the $(-\overline{u_1 u_2}\,)$-equation may have significant positive contribution to the Reynolds shear stress. The buoyancy source term $\beta r_1 \Omega_3^2 \overline{t^2}$ in the $(-\overline{u_1 t})$-equation may have an additional contribution through the Coriolis source term $2\Omega_3 \overline{u_1 t}$ in the $(-\overline{u_2 t})$-equation. However this latter effect, if significant, must be dependent on the direction of rotation, being contradictory to the present results. Thus it may be inferred that the effect of centrifugal buoyancy shown in Fig. 9 has mainly resulted from the centrifugal buoyancy source of Reynolds shear stress $\beta r_1 \Omega_3^2 \overline{u_2 t}$. It is interesting to note that the opposite effect is possible for a cooled wall, where $\overline{u_2 t}$ is negative.

5. Conclusions

When the Coriolis force acts toward the wall, heat transfer in a laminar boundary layer is dramatically enhanced. This can be explained by the generation of streamwise vortices by Coriolis torque and resulting enhancement of the transverse convection of energy. The turbulent heat transfer is slightly enhanced by the wallward Coriolis force, which may be attributed to the elevated turbulent diffusion through the modifications of turbulent eddies by system rotation.

For the opposite direction of rotation, Coriolis force stabilization exhibits no systematic effect on a laminar heat transfer, while it causes the slight decrease in heat transfer coefficient in a turbulent boundary layer. The latter may be the indirect consequence of the Coriolis sink in Reynolds shear stress equation.

The centrifugal buoyancy enhances the turbulent heat transfer both in pressure and suction side boundary layers. It is suggested that this effect may be due to the modified convection through the buoyancy source term in the Reynolds shear stress equation.

Acknowledgements

The present work has been financially supported by the Ministry of Education, Science and Culture, through Grant-in-aid for Scientific Research, No. 11650189. Dr. M. Matsubara and Mr. Y. Edo are greatly acknowledged for their efforts in constructing the equipment. Miss R. Takagi is also acknowledged for conducting the experiment.

Appendix A

Complete set of Reynolds averaged equations governing incompressible turbulent heat transfer in a rotating reference frame.

Continuity equation

$$\frac{\partial U_l}{\partial x_l} = 0. \tag{A.1}$$

Mean momentum equation

$$\frac{\partial U_i}{\partial \tau} + \frac{\partial (U_i U_l + \overline{u_i u_l})}{\partial x_l} = -\frac{1}{\rho_0}\frac{\partial P}{\partial x_i} + \frac{\partial}{\partial x_l}\left(\nu \frac{\partial U_i}{\partial x_l}\right) - 2\varepsilon_{iilm}\Omega_l U_m + \beta T \frac{\partial \phi}{\partial x_i}. \tag{A.2}$$

Mean energy equation

$$\frac{\partial T}{\partial t} + \frac{\partial (U_l T + \overline{u_l t})}{\partial x_l} = \frac{\partial}{\partial x_l}\left(\alpha \frac{\partial T}{\partial x_l}\right). \tag{A.3}$$

Reynolds stress equation

$$\begin{aligned}\frac{\partial \overline{u_i u_j}}{\partial t} &+ \frac{\partial \overline{u_l u_i u_j}}{\partial x_l} + \overline{u_j u_l}\frac{\partial U_i}{\partial x_l} + \overline{u_i u_l}\frac{\partial U_j}{\partial x_l} \\ &= -\frac{1}{\rho_0}\left(\overline{u_j \frac{\partial p}{\partial x_j}} + \overline{u_i \frac{\partial p}{\partial x_i}}\right) + \nu \frac{\partial^2 \overline{u_i u_j}}{\partial x_l \partial x_l} \\ &\quad - 2\left(\varepsilon_{ilm}\Omega_l \overline{u_m u_j} + \varepsilon_{jlm}\Omega_l \overline{u_m u_i}\right) \\ &\quad + \beta\left(\overline{u_j t}\frac{\partial \phi}{\partial x_i} + \overline{u_i t}\frac{\partial \phi}{\partial x_j}\right).\end{aligned} \tag{A.4}$$

Turbulent heat flux equation

$$\frac{\partial \overline{u_i t}}{\partial t} + \frac{\partial U_l \overline{u_i t}}{\partial x_l} + \frac{\partial \overline{u_l u_i t}}{\partial x_l} + \frac{\partial \overline{u_l u_i} T}{\partial x_l} = -\frac{1}{\rho_0} t \frac{\overline{\partial p}}{\partial x_i} + \nu t \frac{\overline{\partial^2 u_i}}{\partial x_l \partial x_l} - 2\varepsilon_{ilm}\Omega_l \overline{u_m t} + \beta \overline{t^2} \frac{\partial \phi}{\partial x_i} + \alpha u_i \frac{\overline{\partial^2 t}}{\partial x_l \partial x_l}. \quad (A.5)$$

In the above equations, the centrifugal force potential ϕ is defined as

$$\frac{\partial \phi}{\partial x_i} = \varepsilon_{i3k}\varepsilon_{k3m}\Omega_3^2 r_m. \quad (A.6)$$

References

Crane, R.L., Sabzvari, J., 1989. Heat transfer visualization and measurement in unstable concave-wall laminar boundary layers. ASME J. Turbomach. 111, 51–56.

Edo, Y., Obi, S., Masuda, S., 2000. Heat transfer experiments in rotating boundary layer flow. Int. J. Heat Fluid Flow 21, 684–692.

Klebanoff, P.K., 1955. Characteristics of turbulence in a boundary layer with zero pressure gradient. NACA Report.

Lighthill, M.J., 1950. Proc. R. Soc. A 202, 359.

Liu, J.T.C., Lee, K., 1995. Heat transfer in a strongly nonlinear spatially developing longitudinal vorticity system. Phys. Fluids 7 (3), 559–599.

Masuda, S., Hori, D., Matsubara, M., 1994. Secondary instability associated with streamwise vortices in a rotating boundary layer. In: Kobayashi, R. (Ed.), Laminar–Turbulent Transition. Springer, Berlin, pp. 69–76.

Matsubara, M., Alfredsson, H., 1996. Experimental study in rotating channel flow. Phys. Fluids 8, 2964–2973.

Morris, W.D., Ayhan, T., 1979. Observation on the influence of rotation on heat transfer in the coolant channels of gas turbine blades. Proc. Inst. Mech. Eng. 193, 303–311.

Reynolds, W.C. et al., 1958. NACA Mem. 12-2-58W.

Saric, W.M., 1994. Goertler vortices. Ann. Rev. Fluid Mech. 26, 379–409.

Toe, R., Ajakh, A., Peerhossaini, H., 2001. Heat transfer in transition to turbulence by goertler instability. In: Proceedings of Turbulent Heat Transfer II, Alaska, 2001 (CD-ROM).

Wagner, J.H., Hohnson, B.V., Hajak, T.J., 1991. Heat transfer in rotating passages with smooth walls and radial outward flow. ASME J. Turbomach. 113, 42–51.